# BLOCK BUNDLE ADJUSTEMENT OF LANDSAT-7 ETM$^+$ IMAGES OVER MOUNTAINOUS AREAS

Thierry Toutin

Natural Resources Canada, Canada Centre for Remote Sensing

588 Booth Street, Ottawa, Ontario, Canada, K1A 0Y7

thierry.toutin@ccrs.nrcan.gc.ca

Generation of image block with Landsat-7 ETM$^+$ imagery and evaluation of block bundle adjustment with reduced number of GCPs

**KEY WORDS**

Block bundle adjustment, Landsat-7 imagery, Geometric evaluation, Error propagation

**ABSTRACT**

*This research study showed the potential of block bundle adjustment with nadir viewing sensor images, such as Landsat-7 ETM$^+$. The method is based on the 3D analytical geometric model developed for multi-sensor images at the Canada Centre for Remote Sensing, Natural Resources Canada. Different block sizes and configurations were tested and compared using image bundle adjustment. The different tests using fifteen Landsat-7 ETM$^+$ images (five paths and three rows) acquired over a study site in the Canadian Rocky Mountains, showed that the same results (around 25 m errors) could be obtained with image blocks as with a single image using a largely reduced number of ground control points (GCPs). However, the combined image measurement and map errors of GCPs were included in the final error budget and the internal accuracy of the blocks should be better (around one pixel or less). The number of GCPs to be used depended mainly on the cartographic data accuracy: more GCPs than the minimum required reduced the error propagation in the least-squares block bundle adjustment. In addition, tie points with a known elevation value (elevation tie points, ETPs) instead of normal tie points were used to link the adjacent images/strips (North-South and East-West) because the viewing-angle differences of overlapping images were smaller than 1° in North-South overlaps and around 10° in East-West overlaps. Better and more consistent results were also obtained using strips of images in the blocks acquired from the same orbit and date instead of using independent images. Finally, using*

*only GCPs in the outer strips/images and ETPs in each overlap achieved the same results (25-m errors).*

## 1. INTRODUCTION

As in photogrammetry where strips and blocks of aerial photos are processed together when no or few ground data is available, the same process can be applied with satellite images from the same and/or adjacent orbits, thus performing the geometric processing with a block bundle adjustment instead of a single image bundle adjustment. There are different advantages to the block bundle adjustment:

- The number of ground control points (GCPs) is largely reduced;
- All image geometric models are computed together;
- A homogeneous digital elevation model (DEM) can be generated when the block has a full and good stereo coverage;
- A better relative accuracy between the images can be obtained;
- A more homogeneous and accurate ortho-mosaic over large areas can be obtained; and
- A homogeneous GCP network for geometric processing can be generated.

This block bundle adjustment process was first developed and scientifically tested with French SPOT across-track stereo images (Toutin, 1985; Veillet, 1991) and with German MOMS along-track stereo images (Kornus *et al.*, 2000). While Landsat block images were also processed with commercial software to create a mosaic over large areas with 50-m accuracy (Earth Satellite Corporation, 2000), few or no scientific results addressed the conditions of experimentation with nadir viewing images, such as from Landsat 7, where the intersection geometry between adjacent images is weak (intersection angles less than 15°). However, the block adjustment process with Landsat images can only be used for ortho-mosaicking with existing DEMs and not for generating DEMs, such as with stereo air photos or MOMS stereo images, because full stereo coverage cannot be generated with such nadir viewing images.

This paper will further investigate the block bundle adjustment with Landsat-7 $ETM^+$ images acquired over the Canadian Rocky Mountains. Firstly, the method to generate and process image strips and blocks using Landsat-7 $ETM^+$ images are presented. The processing of different strips and blocks using

different numbers and distributions of GCPs are then addressed and result comparisons enabled the accuracy of the system and its stability to be evaluated.

The mathematical tool used is the 3D analytical geometric correction model developed for SPOT data (Guichard, 1983; Toutin, 1983), adapted to multi-sensor images (Toutin, 1995) and recently to Landsat-7 ETM$^+$ images (Cheng *et al.*, 2000) at the Canada Centre for Remote Sensing (CCRS), Natural Resources Canada. To compute the model parameters of all images together, an iterative least-squares method using ground control and orbit information is used for the block bundle adjustment. With the block bundle adjustment, the same number of GCPs is needed as for a single image. For an image, strip or block, six GCPs are enough for Landsat-7 imagery (Cheng *et al.*, 2000). Practically, a larger number of GCPs will reduce the propagation of GCP errors (identification, image measurement and map) in the geometric models due to a larger equation redundancy in the least-squares adjustment.

## 2. GENERATION OF STRIPS AND BLOCK

### Image-strip generation

Since satellite data are acquired in a continuous strip the data should be delivered in such long strip depending upon the user's requirements. However, the strips are in general "artificially" cut into square images with overlap areas. Consequently, the images from the same orbit and from the same acquisition date must be stitched together to recreate the continuously acquired strip. Landsat-7 ETM$^+$ images are generally geo-referenced level 1G data, which are corrected for systematic distortions and projected along the ground orbit path at the image centre. This orbit-path projection generates a different azimuth related to the cartographic North for each consecutive image of the same orbit. Consequently, the image lines in the overlap area do not superimpose any more. Using information in the overlap area, the rotation-translation between two consecutive images can be computed with visual or automatic processing techniques to stitch images into a strip (Sakaino *et al.*, 2000). Stitching were checked on different strips and less-than-half pixel errors were noticed. However, long strips could also be directly ordered from ground receiving stations to avoid the stitching.

Theoretically, there is no limit to the number of images that can be stitched or ordered when acquired on the same date, but practically cloud coverage is a limiting factor. In fact, no more than three images

from the same orbit with less than ten percent of clouds were found for our study site over a three-year period. When images are acquired from different dates and thus from different physical orbits, they cannot be stitched in the same image strip. A method using tie points (TP) to create a planimetric link between North-South images must be applied. Due to orbit maintenance of a few kilometers and a satellite altitude of approximately 700 km, the geometry of intersection is very weak with base-to-height (B/H) ratio around $10^{-3}$. Since B/H ratios of 0.6 to 1.0 are needed for a good stereo intersection (Light *et al*., 1980), a known elevation (*Z*-value) extracted from existing contour lines or DEMs should be added to TPs (elevation tie points, ETPs) to strength the intersection geometry between the two images and the Earth as well as to reduce the planimetric error in ETP *Z*-elevation plane.

**Image-block generation**

Blocks of images can be generated from images or strips in the East-West direction acquired from adjacent orbits. The link between adjacent images/strips is also realized with TPs. Since Landsat imagery are acquired at nadir with a 15° field of view, the intersection angles between adjacent images are about 7° to 14° depending upon latitude, generating B/H ratios of 0.10 to 0.25 (Simard, 1983). As for image strip generation, ETPs should be used in the East-West overlap of adjacent images due to B/H ratios smaller than 0.6, but some TPs could also be added.

## 3. EXPERIMENT

**The study site**

The study site is located in the south of the Canadian Rocky Mountains (from 49° N to 53° N and from 116° W to 122° W) from Vancouver in the south-west to Edmonton in the north-east. This area is characterized by a rugged topography with elevation ranging from 400 m to 4000 m. Land cover consists mainly of a mixture of coniferous and deciduous trees with patches of agricultural land and clearcut areas. Agricultural fields are found mostly along valleys while clearcut areas, linked by new logging roads, are randomly located. Roads are mainly loose or stabilized surface roads of two lanes or less in the mountains. In the valleys, a few roads are hard surface of two lanes or less. Also are lakes and ponds connected through a series of creeks flowing between steep cliffs.

**The data set**

Fifteen Landsat-7 ETM$^+$ panchromatic images with 15-m pixel spacing acquired over the Canadian Rocky Mountains cover an area of 600 km by 500 km (Figure 1). The images are level 1G products, systematically georeferenced and oriented along the orbit path. They generate a block of five paths and three rows with North-South and East-West overlaps of 10 percent and 40 percent, respectively (Figure 1). The 40 percent overlaps in the East-West direction generate approximately 7-8° intersection angles and B/H of 0.12-0.14. The paths 1, 2 and 3 (from left to right) have two images of the same date (outlined in Figure 1), the path 4 has three images from different dates, and the path 5 has three images of the same date. Consequently, block bundle adjustments with different formations of images and strips can be tested:

- A block formed with only one strip of two or three images (2- or 3-image strip);
- A block formed with three independent images (3-image block from same orbit or adjacent orbits) where there are two overlaps (in North-South for same orbit images and in East-West for adjacent orbit images);
- A block formed with the fifteen independent images (15-image block) where there are twelve East-West overlaps and ten North-South overlaps; and
- A block formed with the four strips and the six remaining independent images (4-strip/6-image block) where there are eleven East-West overlaps and five North-South overlaps.

Cartographic data used were 350 topographic maps at 1:50,000 scale with 25 to 30 m accuracy in planimetry and 10 to 20 m in elevation. About fifty-five ground points per image were manually collected, which cover the full elevation range in order to avoid extrapolation not only in planimetry but also in elevation. The measurement errors on the images are one to two pixels (15 to 30 m) in the lowest relief and one to three pixels (15 to 45 m) in the highest relief.

**The CCRS 3D analytical multi-sensor geometric model**

The CCRS 3D analytical geometric model was originally developed to suit the geometry of push-broom scanners, such as SPOT-HRV, and have also benefited from theoretical work in celestial mec

hanics to better determine the satellite's osculatory parameters over long orbit (Toutin, 1983; 1985). The model was subsequently adapted as an integrated and unified geometric modelling to geometrically process multi-sensor images (Toutin, 1995) and further adapted to Landsat-7 imagery

(Cheng *et al.,* 2000). The geometric modelling is integrated because in the final equations, which represents the well-known collinearity condition, it takes into account the different distortions relative to the global geometry of viewing, i.e.:

- the distortions relative to the platform (position, velocity, orientation),
- the distortions relative to the sensor (orientation angles, instantaneous field of view, detection signal integration time),
- the distortions relative to the Earth (geoid-ellipsoid including elevation), and
- the deformations relative to the cartographic projection (ellipsoid - cartographic plane).

In summary, the collinearity equations of a ground point are first written in the instrumental reference system and converted into the cartographic projection system using elementary transformations (rotations and translations), which are functions of the parameters describing the distortions previously mentioned (Toutin, 1983). The 3D analytical model integrates the following transformations:

- rotation from the sensor reference to the platform reference;
- translation to the Earth's centre;
- rotation which takes into account the platform time variation;
- rotation to align the z-axis with the image centre ($M_O$) on the ellipsoid;
- translation to the image centre ($M_O$);
- rotation to align the y-axis in the meridian plane;
- rotation to have $xM_O$ *y* tangent to the ellipsoid;
- rotation to align the *x*-axis in the image scan direction; and
- rotation-translation into the cartographic projection.

The integration of the different distortions and the derivation of the equations and of the parameters can be found in Toutin, (1983), but the final results for Landsat-7 $ETM^+$ images, which link the 3D cartographic coordinates to the image coordinates is given by:

$$Pp + y\,(1 + \delta\gamma X) - \tau h = 0 \qquad (1)$$

$$X + \theta\, h/\cos\chi + \alpha q(Q + \theta X - h/\cos\chi) = 0 \qquad (2)$$

where $$X = (x - ay)(1 + h/N_o) + by^2 + cxy \qquad (3)$$

Each parameter is given using a mathematical formula (Toutin, 1983) that represents the physical realities of the full viewing geometry (satellite, sensor, Earth, map projection):

| | |
|---|---|
| $N_o$ | is the normal distance to the ellipsoid; |
| a | is mainly a function of the non-perpendicularity of axes; |
| α | is the instantaneous field-of-view; |
| p, q | are the image coordinates; |
| P, Q | are the scale factors in along-track and across-track directions, respectively; |
| τ and θ | are a function of the leveling angles in along-track and across-track directions, respectively; |
| *x*, *y* and *h* | are the 3D ground coordinates; |
| b, c, χ, δγ, | are 2nd-order parameters, which are functions of the total geometry, e.g., satellite, image and Earth. |

Each of these parameters is in fact the combination of several correlated variables of the viewing geometry, so that the number of unknown parameters has been reduced to an independent uncorrelated set. As examples of combinations of several variables, we have:

- the orientation of the image is a combination of the platform heading due to orbital inclination, the yaw of the platform, the convergence of the meridian;
- the scale factor in along-track direction is a combination of the velocity, the altitude and the pitch of the platform, the detection signal time of the sensor, the component of the Earth rotation in the along-track direction; and
- the leveling angle in the across-track direction is a combination of platform roll, the viewing angle, the orientation of the sensor, the Earth curvature; etc.

This 3D analytical geometric model has been applied to airborne or spaceborne visible and infra-red

(VIR) data (Landsat 5 & 7, SPOT, IRS, ASTER, KOMPSAT, EROS, IKONOS and QuickBird), as well as airborne or spaceborne radar data (ERS, JERS, SIR-C and RADARSAT) with three to six GCPs. This 3D analytical multi-sensor geometric model applied to different image types is robust and not sensitive to GCP distribution as soon as there is no extrapolation in planimetry and elevation (Toutin, 1995). Based on accurate GCPs, the internal accuracy of this model is within one-third of a pixel for medium-resolution images, better than one pixel for high-resolution images and one resolution cell for radar images.

**The processing steps**

Because block bundle adjustments applied to satellite imagery is already documented (Light *et al.*, 1980), the three main processing steps of block bundle adjustments before accuracy evaluation are only summarized:

(1) Acquisition and pre-processing of the Landsat-7 $ETM^+$ images and metadata to determine an approximate value for each parameter of 3D analytical geometric models;

(2) Acquisition of ground points (2D image and 3D cartographic coordinates) and ETPs (2D image and elevation coordinates);

(3) Computation of the block bundle adjustment initialized with the approximate parameter values and refined by an iterative least-squares adjustment with the GCPs/ETPs. Eleven of the previously mentioned parameters (translations, rotation, scale factors, levelling angles, obliquity and some $2^{nd}$ order) were refined in the adjustment within a fixed range using orbital constraints. Each image point for a GCP used the colinearity equations, and each ETP/TP used the coplanarity equations, which are derived from colinearity equations, to set up the error equations (Toutin, 1985). ETPs enable an increase in the relative accuracy between the images and a relative link with the ground. The points (GCPs and ETPs) with fixed coordinates were weighted as a function of their accuracy (cartographic and image coordinates) to set up the normal equations.

Although six accurate GCPs are enough to establish the exact spatial position and orientation of each Landsat-7 $ETM^+$ image or strip, approximately fifty-five points and twenty ETPs to link the images were collected for each image. A larger number of points enabled the propagation of image measurement and map errors in the least-squares bundle adjustment computation of 3D analytical

models to be reduced due to a large equation redundancy, as well as it enabled accuracy tests with Independent Check Points (ICPs) to be performed.

**The block bundle adjustment tests**

Three sets of block bundle adjustments were performed with the data set by varying the number of images and strips in the block and the number and distribution of GCPs used in the bundle adjustment:

1. All points were used as GCPs for one or two independent image(s), for strips with two or three images (2- or 3-image strips), for blocks with three images (3-image blocks) in North-South or East-West directions, and finally for the whole block with the fifteen images (15-image block) or with the four strips and the six remaining images (4-strip/6-image block);
2. A limited number of GCPs were used for blocks with three images (3-image blocks) in North-South or East-West directions. The GCPs were located on the outer images only and ETPs in the two image overlaps; and
3. A limited number of GCPs were used for the block with the fifteen independent images (15-image block) or the block with four strips and six images (4-strip/6-image block). Two different GCPs configurations were tested: (a) GCPs every second images or strips (such as checkerboard) and (b) GCPs on the outer images or strips. ETPs were also used in each image overlap.

The results on one or two independent images in the first tests are used as reference for comparison with the block bundle adjustment results. In addition, before performing the set of tests 2 and 3, different GCP/ICP configurations using the 3-image long strip (the most Eastward strip), which had 148 GCPs, were evaluated to find the optimal reduced number of GCPs in relation to the error of the cartographic coordinates.

## 4. RESULTS AND INTERPRETATION

**All points are used as GCPs**

Table 1 gives the root mean square (RMS) and minimum/maximum residuals (in meters) of these different tests where all GCPs were used in the block bundle adjustment of: one or two independent image(s), the 2- or 3-image strips, the 3-image blocks in North-South or East-West directions, the 15-image block and the 4-strip/6-image block. The results for one or two independent images were used

as reference for comparison of the other strip/block bundle adjustment results. The results for each test (image(s) or strips) correspond to the mean of results for all possibilities for the test (e.g., the result for one or two independent images is the mean result of 15 single images). In the block bundle adjustments, GCPs (colinearity condition) belonging to more than one image were also used as TPs (coplanarity condition). With the 3D analytical geometric model, the residuals do not reflect the modelling accuracy but rather the error of the input data when there are more GCPs as the minimum required (Toutin, 1995). In fact, Table 1 shows that the RMS residuals are slightly smaller than the combined image measurement and map accuracy of GCPs.

All tests with more than one image gave approximately the same results than the reference test with one or two image(s): more or less 20 m in both axes with minima/maxima residuals less than three times the RMS residuals. Because these residuals included the 25- to 30-m map errors of GCPs, the internal accuracy of all block adjustments is thus better (in the range of pixel or less) and these results were then consistent with previous results (7-m accuracy) using accurate GCPs (Cheng *et al.*, 2000). Although non-significant, the RMS residuals for the 15-image block were a little better than the RMS residuals for the 4-strip/6-image block and the RMS residuals for 2 or 3 independent images were a little better than for 2- or 3-image strip residuals. The most probable reason is that the degrees of freedom of the least-squares adjustment are smaller due to more images. Conversely, the minima/maxima residuals are larger because the intersection geometries in the North-South direction are weaker. These coherent results (equivalent RMS, minima and maxima) demonstrate the applicability of the geometric model and of the block bundle adjustment for Landsat-7 $ETM^+$ images, but also show a good stability and robustness of the method over the full image block without systematic and random errors, regardless of the image/strip/block. The use of overabundant GCPs (six is the theoretical minimum) in the least-squares bundle adjustment reduced the propagation of different input data errors (image measurement error of 15 to 45 m and map error of 25 to 30 m) in the 3D analytical geometric model(s), but conversely these input errors are reflected in GCP residuals.

However, unbiased validation of the positioning accuracy has to be realized with ICPs, which were not used in the 3D analytical model calculation. To find the optimal number of GCPs in relation to their errors (image measurement and map) to be used in the bundle adjustments, different tests were performed by varying the number of GCPs/ICPs. The 3-image strip (path 5) was used because it had

the largest number of GCPs (148). Points not used as GCPs were used as ICPs to verify the model and block errors. Figure 2 gives the RMS *X*-*Y* residuals (in meters, lines with squares) when GCPs varied from 148 to 10 in the least-squares strip bundle adjustment, as well as the RMS *X*-*Y* errors (in meters, lines with triangles) for the ICPs varying from 0 to 138. While the RMS *X* residuals/errors (black lines) seem worse than RMS *Y* residuals/errors (white lines), the offsets varying between -1 m and +3 m was not significant. Furthermore, the maximum variations of ICP RMS errors (lines with triangles) were only 3 m and 4 m for each axis: approximately 24 m to 27 m for *X* and 21 m to 25 m for *Y*. Since 3 to 4 m variation was not very significant, the geometric model is then not sensitive to GCP number, even for strips more than 500-km long. In addition, these results were similar to those obtained with one or two independent images.

Since ten GCPs give RMS errors 20% worse than using 30 to 130 GCPs (with only 2 to 3 m variations), 25 to 30 GCPs are then a good compromise for this data set to avoid the propagation of GCP errors and to keep the block error below 25 m in the least-squares bundle adjustment. As mentioned before, the internal accuracy of the strip is better because the errors of ICPs are included in the 25-m error budget.

**Limited number of GCPs for 3-image block**

The previous result with 25 GCPs was then applied to test small blocks generated with 3 images in North-South direction from same paths but from different dates (Figure 3), and in East-West direction from different paths and dates (Figure 4).

Preliminary tests were performed using only TPs in the image overlaps. The results for the two 3-image blocks depending on the number and distribution of the TPs were inconsistent with RMS errors varying from 30 m to hundreds of meters. Depending on the TP quality, the error propagated differently in the inner image due to very weak B/H ratios. These inconsistent results confirmed that ETPs have to be used to avoid the error propagation of TP image measurement as well as to strengthen the link between the images and the ground. Figures 3 and 4 show the results with 10 to 20 ETPs in each overlap: the left window with the GCPs (circles) and ETPs (squares) distribution and the right window with the ICP error vectors. Table 2 (upper two lines) also shows the number of GCPs/ETPs/ICPs, GCP RMS residuals and ICP RMS errors for the two tests.

The results were better for East-West 3-image block than for North-South 3-image block because B/H ratio was much larger. For the two tests, GCP RMS residuals (18 to 23 m) were approximately in the same order of magnitude as the RMS residuals (19 to 21 m) for the reference image (Table 1) when using all GCPs. In addition, since ICP RMS errors (25 m) were approximately to the same order as ICP RMS errors (22 to 25 m) of Figure 2, it confirmed that 25 GCPs were appropriate to reduce the error propagation. Since RMS residuals/errors included the input data errors (image measurement of 15 to 45 m and map of 25 to 30 m), the internal accuracy of the 3-image block is better than 25 m. By computing separately the RMS errors on ICPs for each image, one obtained that the inner image errors are slightly larger (10 to 15 percent) than the outer image errors, showing that the ETPs "transferred the information" in the block bundle adjustment. The analysis of ICP vector errors (Figures 3 and 4) confirmed this statement and in addition showed there were no systematic or local errors in any of the three images.

**Limited number of GCPs for the whole image block**

The block bundle adjustments were now performed with the 15-image block and the 4-strip/6-image block: (a) with 25 GCPs every second images or strips ("checkerboard" configuration) (Figures 5 and 6); and (b) with 25 GCPs only in the outer images or strips (Figures 7 and 8).

For clarity, Figures 5 through 8 only showed the ICP error vectors due to the large number of points. The images with dashed lines are the images without GCP. ICP vectors are the differences between the known and the computed cartographic coordinates for each image point. ICPs belonging to more than one image have thus an error vector for each image: the closer are these error vectors, the smaller is the relative error between the different image points projected on the ground and the better is the superposition of the overlapping images. The evaluation on these points is then an indication of how well the block bundle adjustment performed. Figures 5 and 7 are for the results of 15-image block and Figures 6 and 8 are for the results of 6-image/4-strip block. For each test (a), the images without GCPs were linked with approximately ten ETPs on each overlap and five to ten TPs in the East/West overlaps because the North/South overlaps displayed too weak stereo-geometry. Since the tests (b) are the "most extreme case" (no GCPs between 360 to 400 km), fifteen ETPs were used on each overlap (TPs were transformed as ETPs). The number of GCPs/ETPs/TPs/ICPs, the RMS residuals and RMS errors are synthesised in Table 2 (lower four lines).

The general results of Table 2 and Figures 3 to 8 show a general coherency and confirm the results and the interpretation of Table 1 and the previous 3-image block results:

- A general error of 25 to 30 m quite similar to the results of one or two independent images and of strip results and a good relative superposition in the overlap areas;
- The applicability of the model to block bundle adjustment;
- The stability and robustness of the method regardless of image and/or strip configurations in the block; and
- The stability and the robustness of the method regardless of GCP/ETP/TP distributions.

Since ICP RMS errors, as being the error budget, included the 25 to 30 m cartographic errors, the internal accuracy of the block is better (in the order of pixel or less). Unfortunately, accurate checked data (more accurate than 10 m) was not available on this study site to quantify and confirm the final accuracy. The two 15-image block bundle adjustments (Figures 5 and 7) with "the weaker intersection geometry" between consecutive images of the same orbit and date ($B/H \approx 10^{-5}$) give the worst results (30 to 35 m), especially when GCPs are used on the outer images/strips (block b, Figure 7). The comparison of the two block configurations confirms that generating strips from consecutive images of the same orbit and same date enables better and more consistent results to be obtained. Consequently, a block formed with strips instead of independent images should be favoured. An other major advantage is that 3-image strips require three times less GCPs than three independent images, and the reduction factor is proportional to the number of image in the strip. Figures 5 to 8 demonstrate that there is no bias or systematic error in any strip and block bundle adjustment regardless of images and strips with or without GCPs. Statistical evaluations for each image independently confirm this last statement. Furthermore, ICP error vectors for points belonging to two images or more were in the same direction, demonstrating a good relative superposition between the images. Since the results obtained are similar for any image of this block (e.g., image with or without GCPs), there is no local systematic/random error and the block bundle adjustment method performed well in terms of relative and absolute accuracy.

All the tests performed demonstrated that the CCRS 3D analytical geometric model and block bundle adjustment were both stable and robust for Landsat-7 $ETM^+$ images without generating local random or

systematic errors regardless of numbers or distribution of images/strips and GCPs. The tests and results also demonstrated that input GCP errors did not propagate through the rigorous model, but rather was reflected in the residual. The use of an overabundance of GCPs (six is the theoretical minimum) in the least-squares bundle adjustment has reduced the propagation of the input data errors (image measurement and map) in the block modelling. Since GCP residuals were on the same order of magnitude as ICPs errors they can be used, when redundant, as *a priori* mapping error, by taking into account the cartographic data errors. Finally, these results then give a good level of confidence of the applicability and robustness of the CCRS 3D analytical multi-sensor model applied to block bundle adjustment with Landsat-7 ETM$^+$ data for other study sites and data sets. In addition, these 25-m error results are better than the 50-m RMS accuracy obtained with commercial software as mentioned in Introduction (Earth Satellite Corporation, 2000).

## 5. CONCLUSIONS

A method of spatio-triangulation using a block bundle adjustment was tested with fifteen Landsat-7 ETM$^+$ panchromatic level-1G images acquired over the Canadian Rocky Mountains using CCRS 3D analytical multi-sensor geometric model. The least-squares bundle adjustment computed with all GCPs was first tested with independent images, strips and blocks: the results (around 20-m RMS residuals) were similar regardless of the configuration and the number of images, strips and block. In addition, the results were on the same order and even slightly less as the input data errors (image measurement and map). Other test showed that 25 to 30 GCPs were a good compromise to not propagate GCP errors in the 3D analytical models. Using this result, block bundle adjustments were then performed for different block configurations and GCP distributions in the block. All the tests demonstrated the applicability as well as the stability and robustness of the method with nadir viewing images, regardless of the number of images, the
image/strip/block configurations or the GCP/ETP/TP distributions. Since
a final error budget of 25 to 30 m, which included the combined image measurement and map errors, were obtained, the internal accuracy of the block is then better (in the range of pixel or less). These results are twice better than those obtained with commercial software (Earth Satellite Corporation, 2000). Because the results demonstrated that the use of strips from images of the same orbit and same

date achieved better results with a reduced number of GCPs, a block formed with strips instead of independent images should be favoured.

**Acknowledgements**

The author would like to thank the two anonymous reviewers, which improve the papers with their constructive comments. He also would like to thank Mr. Yves Carbonneau of Consultants TGIS inc., Canada for the block bundle adjustment software, Mr. Alexander Berger and Ms. Alexandra Koch of Technische Universität Dresden, Germany and Mr. René Chénier of Consultants TGIS inc., Canada for Landsat-7 ETM$^+$ image processing. The Centre for Topographic Information Sherbrooke, Natural Resources Canada provided the topographic maps.

**References**

Cheng Ph., Toutin, Th., and Tom V., 2000. Unlocking the Potential of Landsat 7 Data, *Earth Observation Magazine*, 9(2):28-31, (last accessed 12 December 2002 at http://www.ccrs.nrcan.gc.ca/ccrs/eduref/ref/bibpdf/4769.pdf/).

Earth Satellite Corporation, 2000. Landsat TM mosaic of Africa, *Photogrammetric Engineering & Remote Sensing*, (66)9:1039, (last accessed 12 December 2002 at http://www.geocover.com/).

Guichard, H., 1983. Etude théorique de la précision dans l'exploitation cartographique d'un satellite à défilement : application à SPOT, *Société Française de Photogrammétrie et de Télédétection*, 90(2:15-26.

Kornus W., Lehner M., and Schroeder M., 2000. Geometric in-flight calibration of the stereoscopic line-CCD scanner MOMS-2P, *ISPRS Journal of Photogrammetry and Remote Sensing*, 55(1):59-71.

Light, D.L., D. Brown, A. Colvocoresses, F. Doyle, M. Davies, A. Ellasal, J. Junkins, J. Manent, A. McKenney, R. Undrejka and G. Wood, 1980. *Satellite photogrammetry*, in Manual of Photogrammetry Chapter XVII, (Bethesda, USA: ASPRS), pp. 883-977.

Sakaino, S., Suzuki H., Cheng P., and Toutin Th., 2000. Updating maps of Kazakhstan using stitched SPOT images, *Earth Observation Magazine*, (9)3:11-13. (last accessed12 December 2002 at http://www.eomonline.com/Common/Archives/March00/toutin.htm/)

Simard, R., 1983. Digital stereo-enhancement of Landsat-MSS data, *Proceedings of the Seventeenth International Symposium on Remote Sensing of Environment*, 09-13 May, Ann Arbor, MI, USA, (Ann Arbor, USA: ERIM), May 9-13, pp. 1275-1281

Toutin, Th., 1983. *Analyse mathématique des capacités stéréoscopiques du satellite SPOT*. Mémoire de DEA, Ecole Nationale des Sciences Géodésiques, Paris, France, 74 p.

Toutin, Th., 1985. *Analyse mathématique des capacités stéréoscopiques du système SPOT,* Thèse de Docteur-ingénieur, Ecole Nationale des Sciences Géodésiques, Paris, France, 163 p.

Toutin, Th., 1995. Multisource data fusion with an integrated and unified geometric model, *EARSeL Advances in Remote Sensing*, 4(2):118-129, (last accessed12 December 2002 at http://www.ccrs.nrcan.gc.ca/ccrs/rd/sci_pub/bibpdf/1223.pdf/)

Veillet, I., 1991. *Triangulation spatiale de blocs d'images SPOT*, Thèse de Doctorat, Observatoire de Paris, Paris, France, 101 p.

Table 1. Results of the different least-squares block bundle adjustment tests for different image, strip and block configurations using all GCPs: root mean square (RMS) and minimum/maximum residuals (in meters) for the GCPs. The numbers of GCPs are approximated and GCPs belonging to more than one image were counted proportionally. *Z*-residuals for ETPs/TPs are not given because they are not useful to evaluate the planimetric quality of a block formed with nadir viewing satellite images.

| **Least-squares block bundle adjustment** | **GCP Number** | **RMS Residuals** X | Y | **Min/Max Residuals** X | Y |
|---|---|---|---|---|---|
| One independent image | 55 | 20.8 | 18.9 | -59/49 | -45/47 |
| Two independent images | 110 | 21.5 | 19.8 | -41/52 | -41/43 |
| 2-image strip | 110 | 23.2 | 22.5 | -35/45 | -49/37 |
| 3-image strip | 165 | 23.0 | 20.6 | -41/48 | -41/44 |
| 3-image block North-South | 165 | 20.0 | 19.2 | -43/48 | -49/44 |
| 3-image block East-West | 165 | 19.8 | 19.5 | -45/46 | -50/48 |
| 15-image block | 800 | 21.2 | 18.9 | -66/63 | -55/62 |
| 4-strip/6-image block | 800 | 22.6 | 21.2 | -59/52 | -49/47 |

Table 2. Results of the different least-squares block bundle adjustment tests (with reference to Figures) for different block configurations using a reduced number of GCPs: root mean square (RMS) residuals (in meters) for the GCPs and RMS errors (in meters) for the ICPs. The numbers of GCPs/ICPs are approximated. Tests (a) and (b) correspond to two different GCP distributions in the blocks: (a) with GCPs every second images or strips ("checkerboard") and (b) with GCPs only on the outer images or strips. *Z*-residuals for ETPs/TPs are not given because they are not useful to evaluate the planimetric quality of a block formed with nadir viewing satellite images.

| **Least-squares block bundle adjustment tests** | **Figure** | **Number of GCPs/ETPs/ TPs** | **RMS Residuals** *X* | *Y* | **Number of ICPs** | **RMS Errors** *X* | *Y* |
|---|---|---|---|---|---|---|---|
| 3-image block North-South | 3 | 50/20/0 | 22.8 | 22.7 | 120 | 25.2 | 25.3 |
| 3-image block East-West | 4 | 50/44/0 | 18.1 | 17.9 | 100 | 27.1 | 26.1 |
| 15-image block (a) | 5 | 200/160/80 | 16.3 | 16.0 | 600 | 28.0 | 23.3 |
| 4-strip/6-image block (a) | 6 | 150/160/80 | 17.4 | 17.5 | 650 | 27.6 | 25.1 |
| 15-image block (b) | 7 | 100/200/0 | 17.4 | 16.4 | 700 | 35.1 | 28.3 |
| 4-strip/6-image block (b) | 8 | 75/265/0 | 17.4 | 18.8 | 725 | 26.0 | 24.7 |

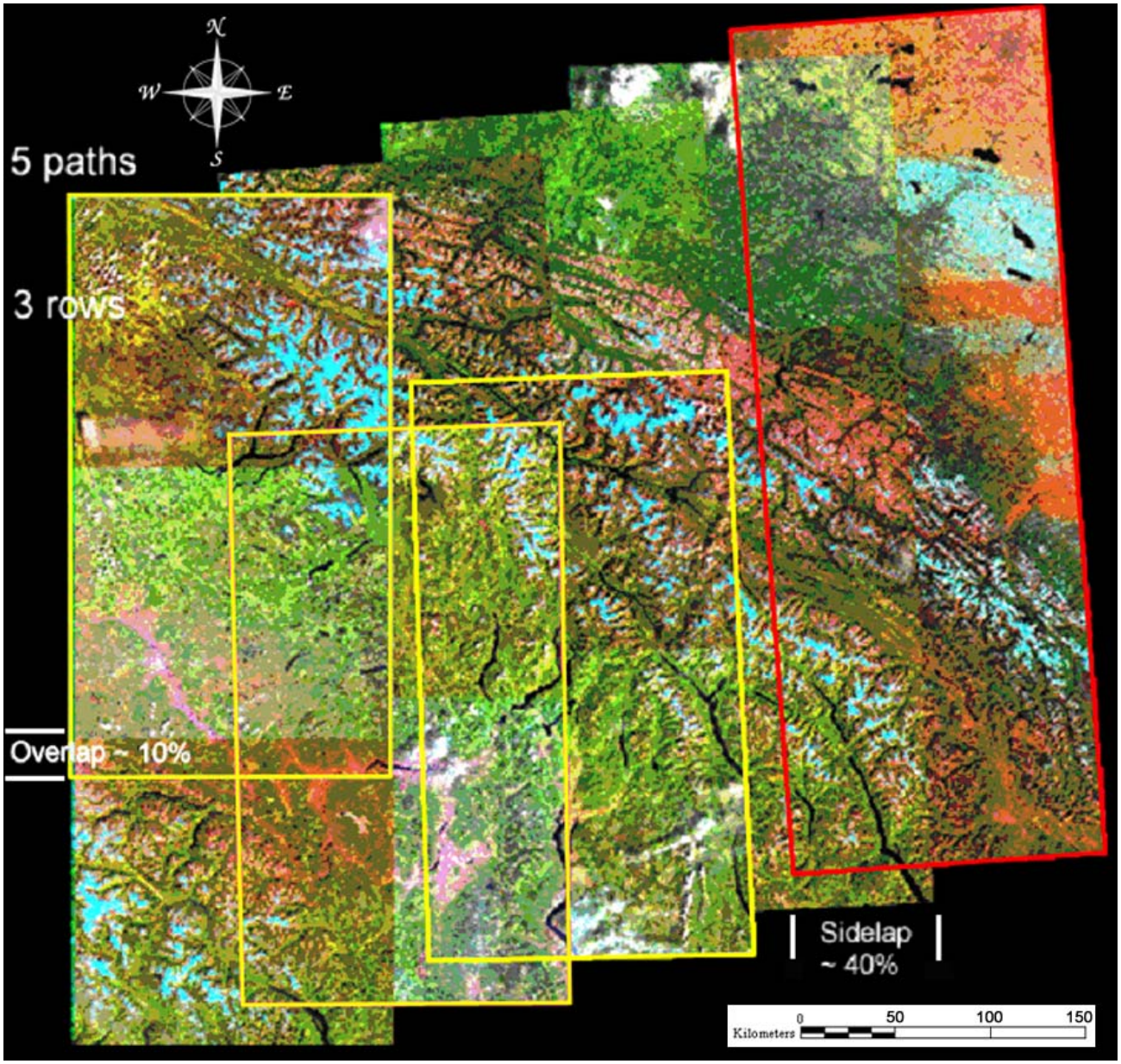


Figure 1. Study site and fifteen Landsat-7 ETM$^{+}$ images (five paths and three rows) over the Canadian Rocky Mountains, Canada. The colored outlines delineate the strips formed with two images (yellow lines) or with three images (red lines) acquired from the same orbit and same date.

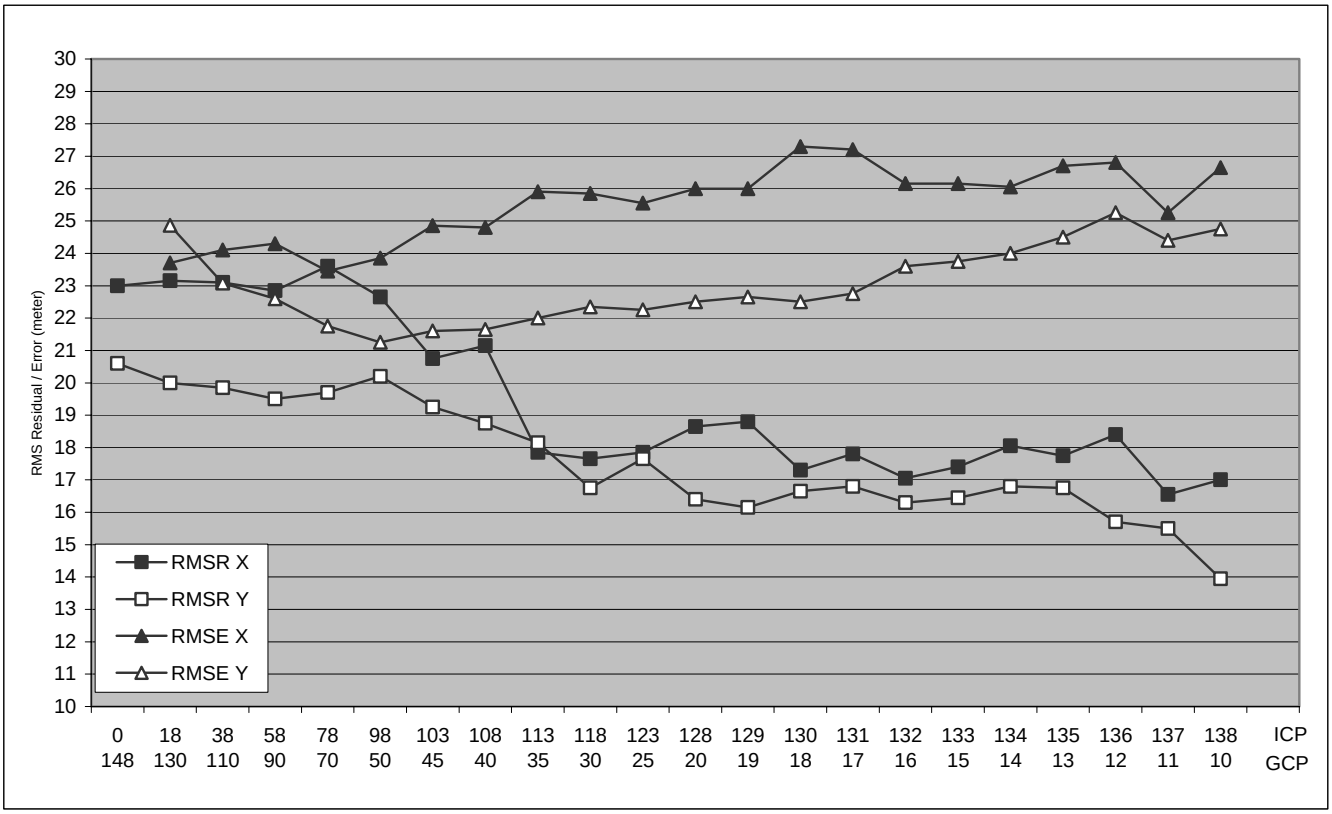


Figure 2. Root mean square *X*-*Y* residuals (RMSR) (in meters) for the GCPs varying from 148 to 10 in the least-squares strip bundle adjustment, and RMS *X*-*Y* errors (RMSE) (in meters) for the ICPs varying from 0 to 138, respectively. *Z*-residuals for ETPs/TPs are not given because they are not useful to evaluate the planimetric quality of a block formed with nadir viewing satellite images.

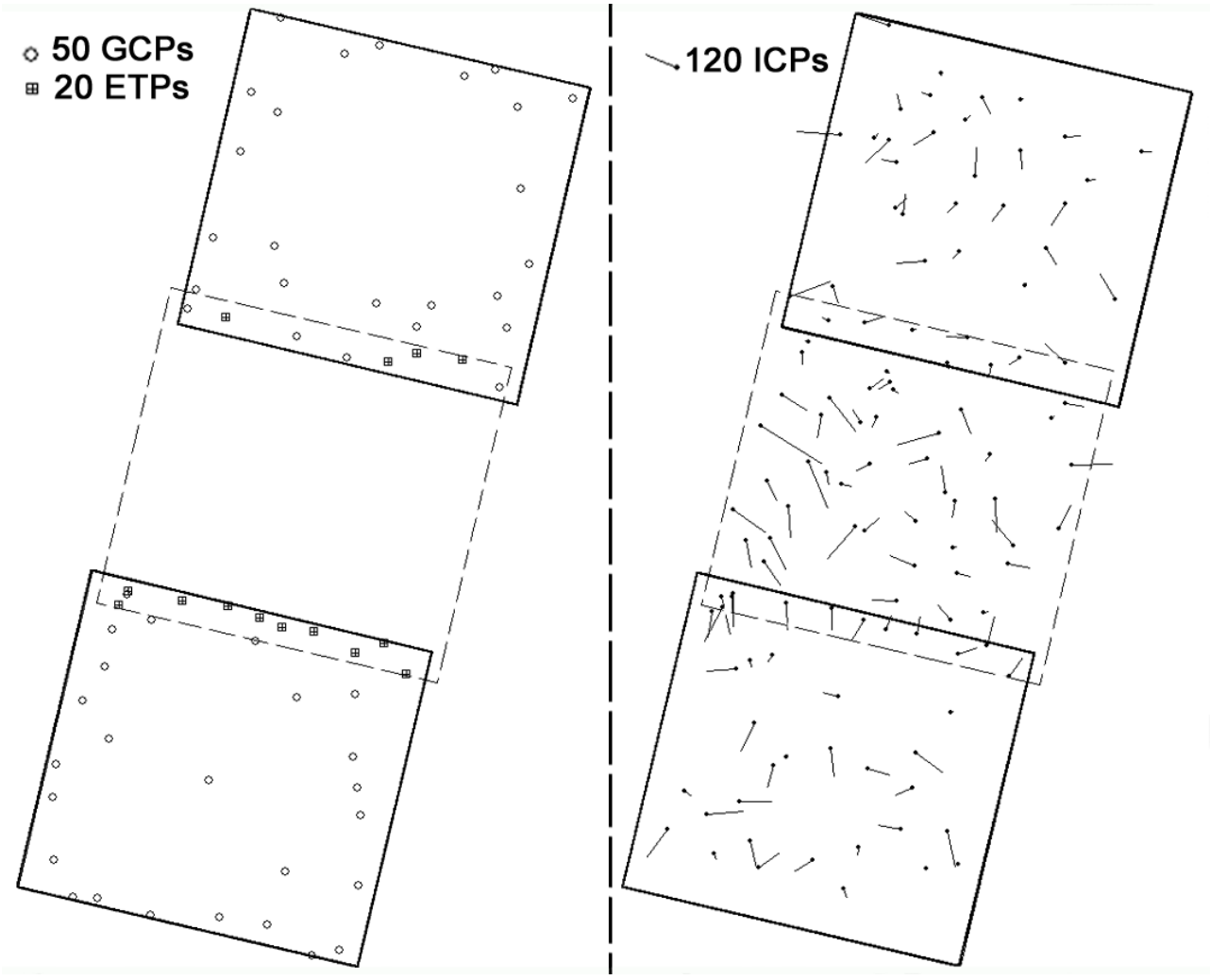


Figure 3. GCP/ETP distribution (left window) and ICP error vectors (right window) of the block bundle adjustment of three images in North-South direction computed with 25 GCPs (circles) on the outer images and 10 ETPs (squares) in each overlap. The images with dashed lines are the images without GCP. ICP vectors are the differences between the "true" cartographic coordinates and the computed cartographic coordinates for each image point.

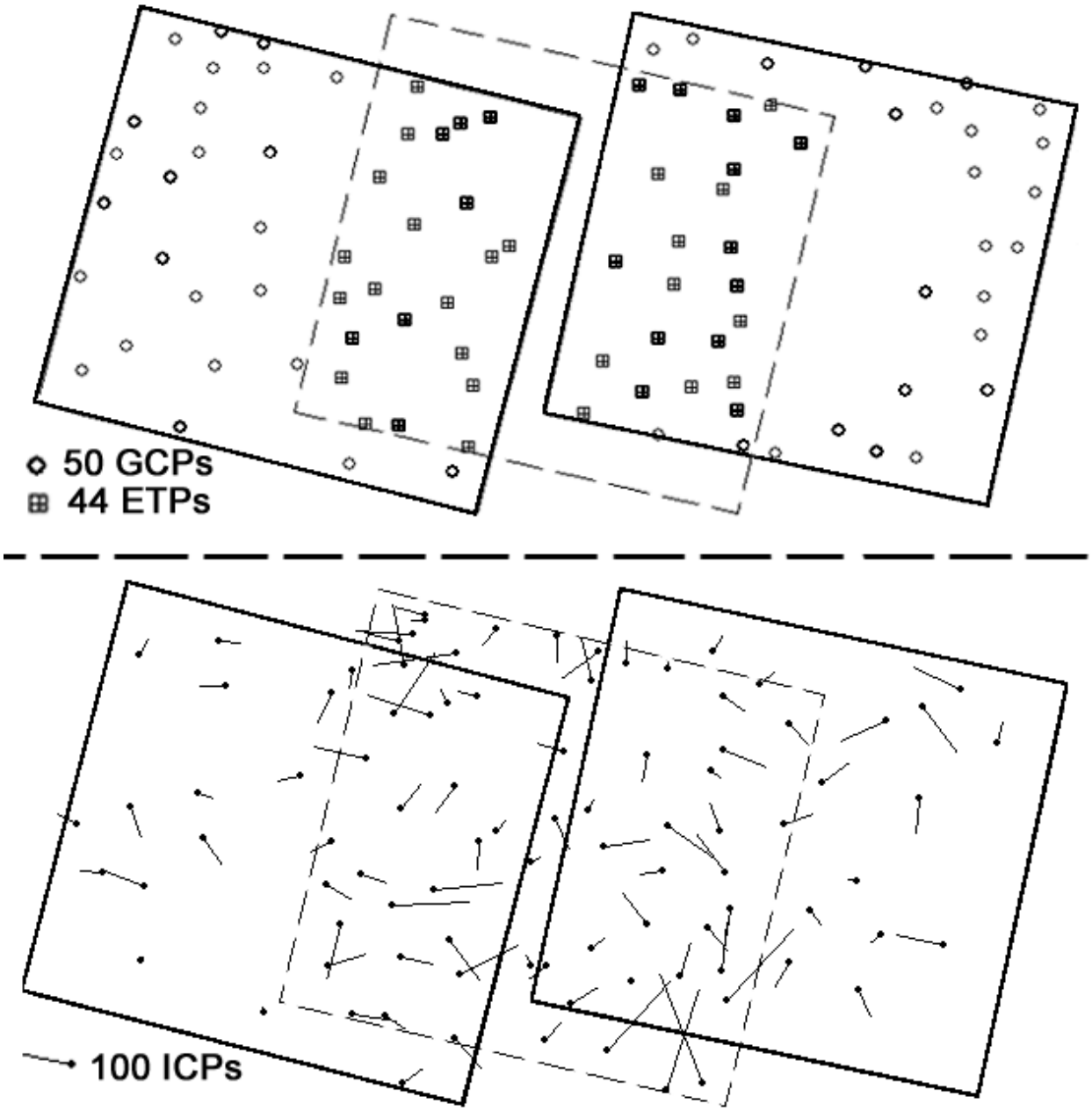


Figure 4. GCP/TP distribution (top window) and ICP error vectors (bottom window) of the block bundle adjustment of three images in East-West direction computed with 25 GCPs (circles) on the outer images and about 20 ETPs (squares) in each overlap. The images with dashed lines are the images without GCP. ICP vectors are the differences between the "true" cartographic coordinates and the computed cartographic coordinates for each image point.

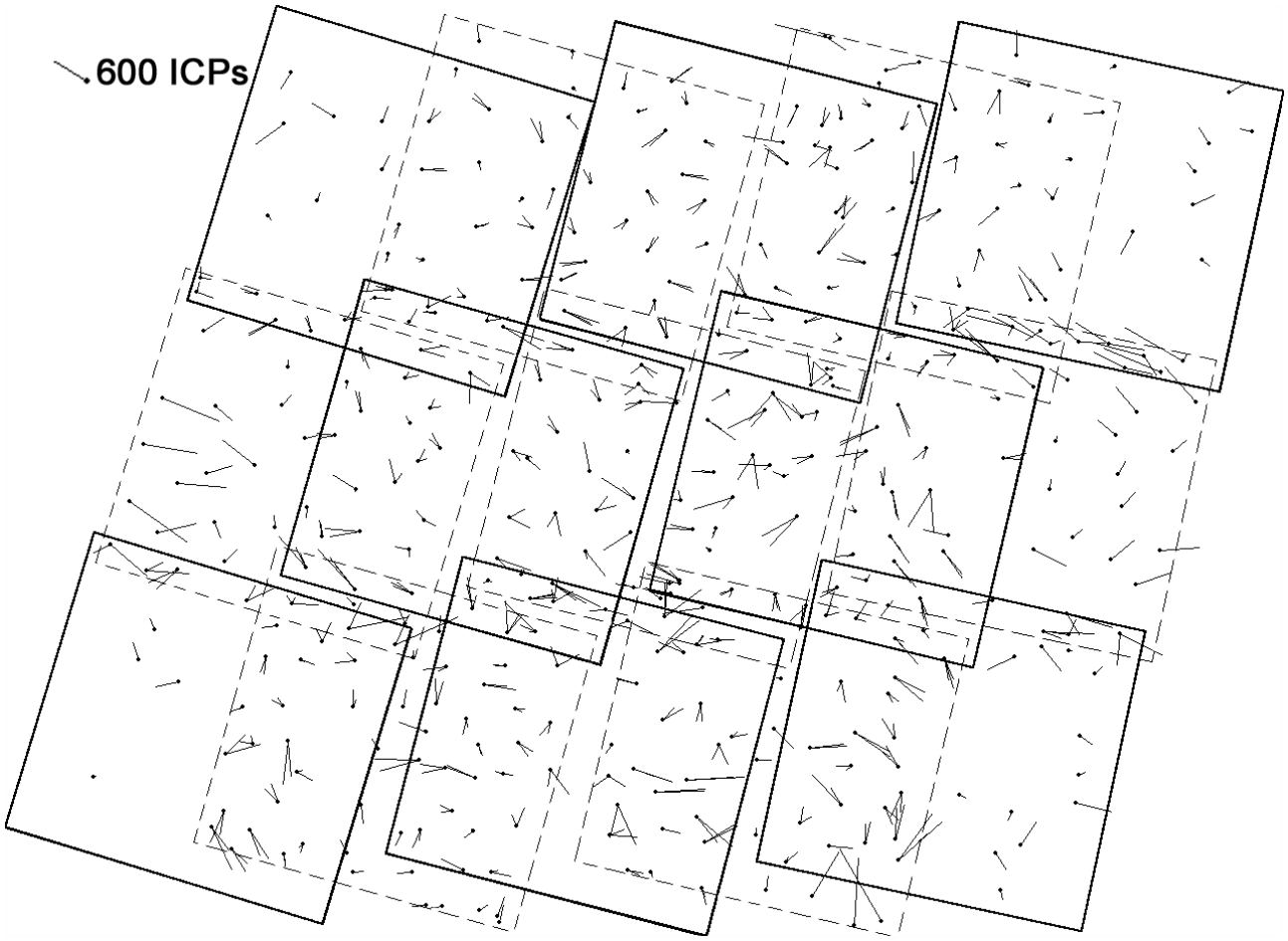


Figure 5.: ICP error vectors of the 15-image block bundle adjustment computed with 25 GCPs every second images ("checkerboard"), about 10 ETPs in each overlap, and in 5-10 TPs in East-West overlap. The images with dashed lines are the images without GCP. ICP vectors are the differences between the "true" cartographic coordinates and the computed cartographic coordinates for each image point. ICPs belonging to more than one image have an error vector for each image: the closer are these error vectors, the smaller is the relative error and the better is the superposition of the overlapping images.

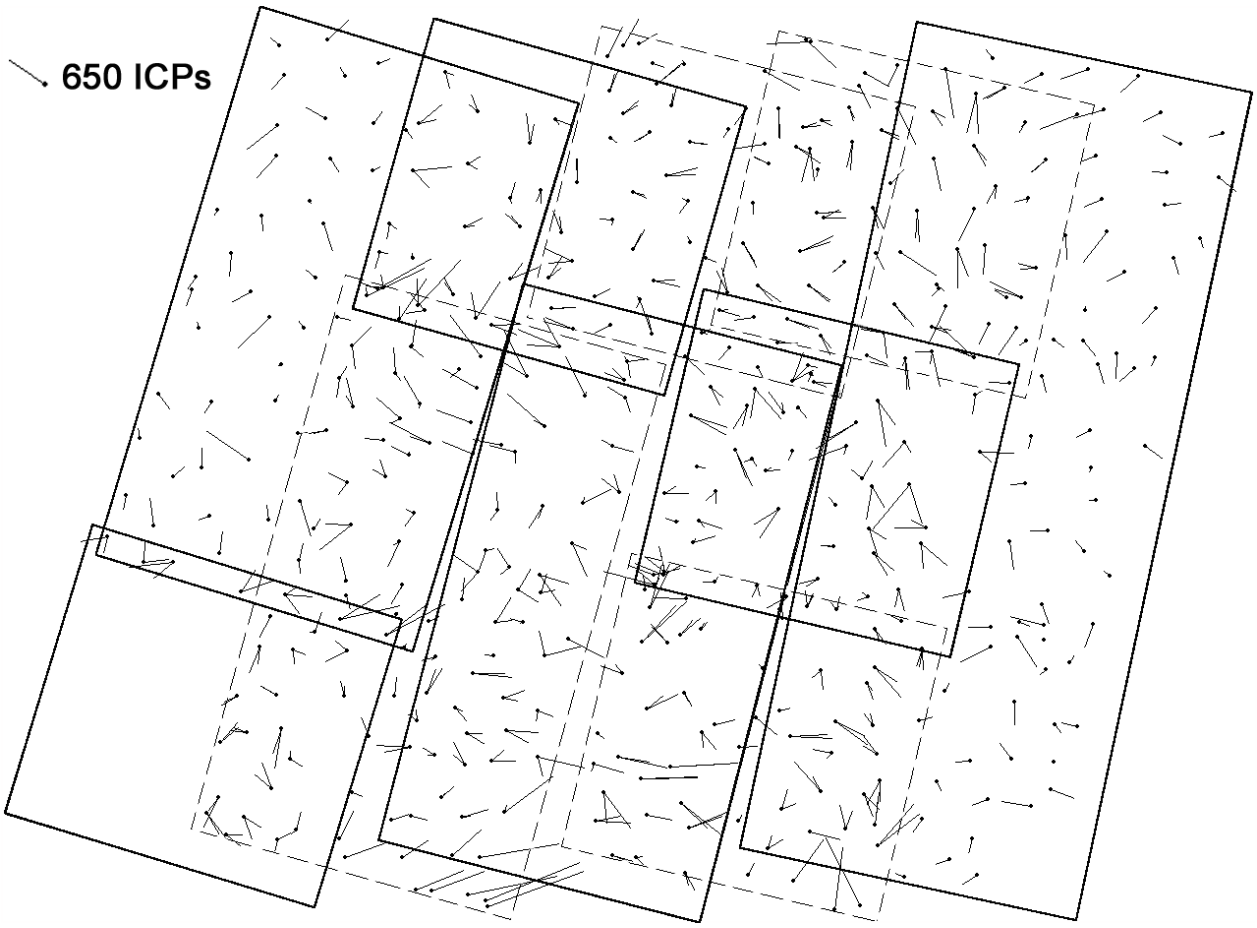


Figure 6. ICP error vectors of the 4-strip/6-image block bundle adjustment computed with 25 GCPs every second images or strips ("checkerboard"), about 10 ETPs in each overlap, and 5-10 TPs in East-West overlap. The images and strips with dashed lines are the images without GCP. ICP vectors are the differences between the "true" cartographic coordinates and the computed cartographic coordinates for each image point. ICPs belonging to more than one image have a error vector for each image: the closer are these error vectors, the smaller is the relative error and the better is the superposition of the overlapping images.

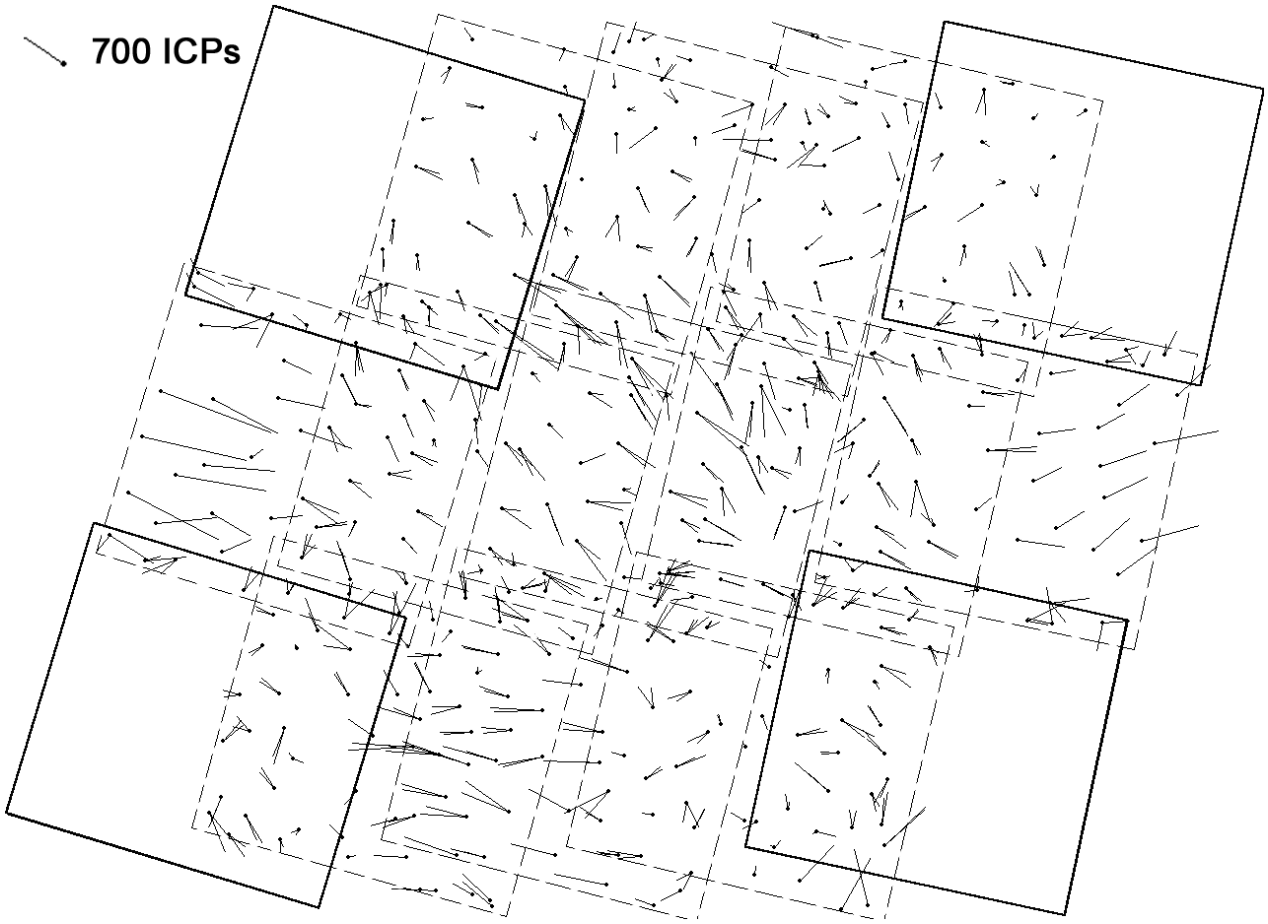


Figure 7. ICP error vectors of the 15-image block bundle adjustment computed with 25 GCPs in the four outer-corner images and about 15 ETPs in each overlap. The images with dashed lines are the images without GCP. ICP vectors are the differences between the "true" cartographic coordinates and the computed cartographic coordinates for each image point. ICPs belonging to more than one image have an error vector for each image: the closer are these error vectors, the smaller is the relative error and the better is the superposition of the overlapping images.


Figure 8. ICP error vectors of the 4-strip/6-image block bundle adjustment computed with 25 GCPs in the three outer image or strips and about 15 ETPs in each overlap. The images and strips with dashed lines are the images without GCP. ICP vectors are the differences between the "true" cartographic coordinates and the computed cartographic coordinates for each image point. ICPs belonging to more than one image have an error vector for each image: the closer are these error vectors, the smaller is the relative error and the better is the superposition of the overlapping images.